JOURNAL OF MATERIALS SCIENCE 23 (1988) 1643–1654

A study on the microstructure and phase transformation of electroless nickel deposits

SU HOON PARK, DONG NYUNG LEE
Department of Metallurgical Engineering, Seoul National University, Seoul, Korea

Electroless Ni–7.4 to 10% P deposits obtained from acidic nickel sulphate baths with sodium hypophosphite as a reducing agent were analysed by transmission electron microscopy, X-ray diffraction and thermal analysis. The deposits could be represented better by a microcrystalline structure composed of 4 to 5 nm fcc Ni–P solid-solution grains rather than an amorphous structure. The deposits also had the (1 1 1) texture, which persisted in nickel grains even after phase separation of nickel and Ni_3P by heating in the case of the low nickel content, whereas the texture approached the random orientation with increasing phosphorus content. The phase transformation temperature was independent of the phosphorus content.

1. Introduction

The electroless nickel deposits using sodium hypophosphite as a reducing agent are binary alloys of nickel and phosphorus [1]. The phosphorus content of the deposits varies with the pH of the solution [2]. The deposits plated from alkaline solution had a lower phosphorus content and were crystalline [3, 4], whereas the deposits from acidic solution had a higher phosphorus content, generally more than 7 wt % P, and were known as amorphous or microcrystalline.

Goldenstein *et al.* [5] in their study of deposits containing 7 to 10 wt % P concluded on the basis of X-ray diffraction and some other considerations that as-plated electroless nickel was amorphous. Makhsoos *et al.* [6–8] studied the microstructure and phase transformation behaviour using transmission electron microscopy (TEM) and *in situ* electron beam heating of electrodeposited Ni–P alloys and found that as-plated deposits containing 12 to 26 at % P were amorphous, and dendritic transformation spread out from the beam centre which might be caused by the nucleation and growth of crystallites from amorphous solid. Some other investigators examined the TEM and interference function for electroless Ni–P deposits and concluded that the deposits had an amorphous-like structure [9–12].

In contrast to these, Graham *et al.* [13] concluded on the basis of electron and X-ray diffraction and some other considerations that as-plated electroless nickel deposits containing 4.6 to 9.4 wt % P were supersaturated solid solutions of phosphorus dissolved in crystalline nickel with numerous stacking faults. Parker [14] also found that crystalline nickel had a (1 1 1) fibrous texture in the as-plated state. Cargill [15] and Dixmier and Duwez [16] studied the X-ray interference function for electrodeposited or electroless plated Ni–P alloys and found a higher degree of short range order than in a liquid.

These conflicting results are thought to be due to the unstable structure of the deposited alloy, and the detailed structures of electroless Ni–P deposits are not well understood. Therefore more basic studies are required to determine whether electroless nickel deposits are microcrystalline supersaturated solid solution or amorphous.

The transformation process from amorphous structure to crystal structure has two stages. First, short-range atomic movements and incipient crystallization of metastable crystalline structures. Secondly, long-range atomic movements cause decomposition to the equilibrium phases. On the other hand, the phase transformation behaviour of microcrystalline supersaturated binary solid-solution alloy has only one transformation process which is very similar to the second stage mentioned above.

The purpose of this work is to study the effect of phosphorus content on the microstructure and the phase transformation behaviour of electroless nickel deposits by using transmission electron microscopy, differential scanning calorimetry and X-ray diffractometry.

2. Experimental procedure

2.1. Electroless nickel plating

To prepare electroless nickel deposits, a 5086 aluminium sheet was used as substrate, nickel sulphate as a nickel source and sodium hypophosphite as a reducing agent. In this study, succinic acid, aminoacetic acid, malic acid and citric acid were used as complexing agents [17], sodium fluoride as an accelerator, and thiourea as an inhibitor.

The chemical composition of the bath which was used in this study to obtain the electroless plated deposit was as follows: 20 kg m^{-3} $NiSO_4 6H_2O$, 20 kg m^{-3} $NaH_2PO_2H_2O$, 26 kg m^{-3} total complexing agent, 300 p.p.m. NaF, 0.5 p.p.m. thiourea and NaOH to adjust the pH of the solution from 4.6 to 5.3. The temperature of the bath was maintained at 87 $\pm$ 1° C with a thermoregulator and nitrogen gas was injected at the bottom of the bath for agitating the plating solution.

To study the effect of phosphorus content on the

0022–2461/88 $03.00 + .12

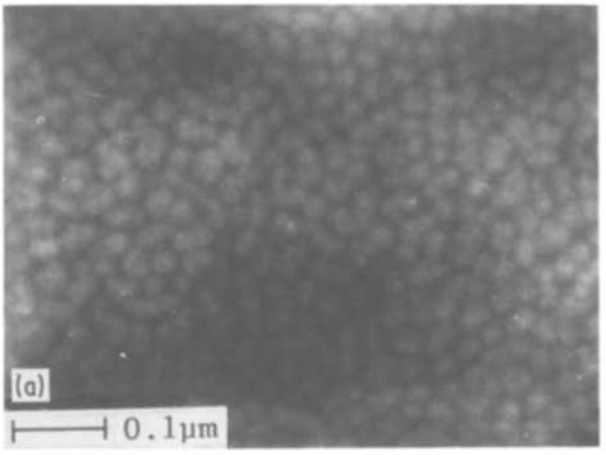

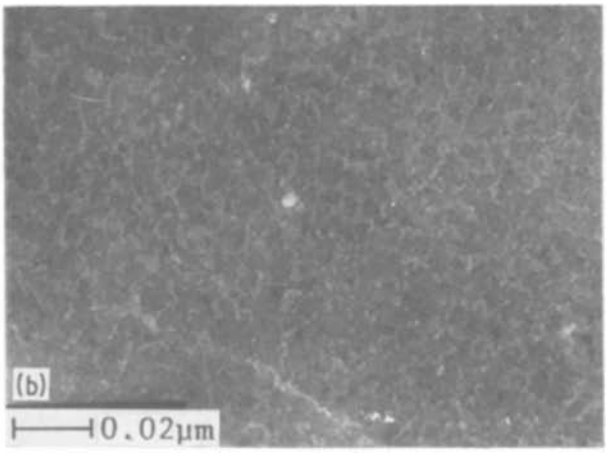

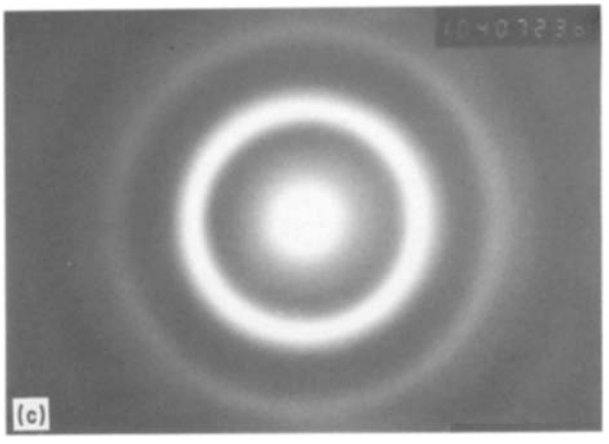

Figure 1 TEM microstructures and diffraction pattern of specimens deposited for 2 h at pH 4.6.

microstructure and phase transformation of electroless Ni–P deposits, deposits with various phosphorus contents were obtained. The parameters which determine the phosphorus content in electroless Ni–P deposits are known to be the nickel and reducing agent concentrations, the type and concentration of inhibitor and accelerator in the plating solution, and the pH and temperature of the solution [18]. Of all these, the pH of the solution is one of the most dominant parameters on the phosphorus content of the deposit. So, we adjusted only the pH of the solution at intervals.

The phosphorus content in Ni–P deposits was analysed by measuring the mass of $Mg_2P_2O_7$. The phosphorus content in the deposits obtained from solutions of pH 4.6, 4.9 and 5.3 is given in Table I.

2.2. Structure analysis

The Ni–P deposits of 30 μm thickness which were obtained by electroless plating for 2 h were peeled from the substrates. The peeled deposits were cut to 3 mm diameter and thinned to 10 μm by mechanical polishing both sides of them, and finally thinned to a suitable thickness for TEM analysis by twin jet polishing. The X-ray diffractometer was used in two ways. To measure the X-ray diffraction pattern the common continuous-scanning method was used, whereas to obtain measured X-ray intensities for calculation of the interference function a step-scanning method was used. For the step scanning, the step width was 0.2° and the counting time for one step was 100 sec. The measured intensity data were corrected and converted to interference function, pair distribution function and radial distribution function [19].

TABLE I Content of phosphorus in electroless nickel deposits obtained from various solutions

pH	Composition			
	P (wt %)	P (at %)	Ni_3P (wt %)*	Ni_3P (vol %)*
4.6	10.07	17.51	67.3	70.1
4.9	9.52	16.62	63.5	66.4
5.3	7.42	13.19	49.6	52.8

*The Ni_3P content was calculated assuming that all phosphorus forms Ni_3P when annealed.

2.3. Phase transformation behaviour

The phase transformation temperature was measured using a differential scanning calorimeter and a differential thermal analyser, at various heating rates. Heat treatment was carried out in a salt bath for various periods of time. After heat treatment the microstructural change and phase transformation behaviour were analysed using TEM and X-ray diffractometer.

3. Results and discussion

3.1. Structure

Figs 1a and b show TEM microstructures of the Ni–P deposits obtained from pH 4.6 solution after 2 h. The microstructure shows a dark network (Fig. 1a) which is often observed in other thin films that are claimed to be amorphous, but shows extremely small grains of 4 to 5 nm diameter when further magnified, the grain boundaries of which are brighter possibly due to their greater etching tendency (Fig. 1b). The dark network has been thought to be due to an inhomogeneous solute distribution. However, its electron diffraction pattern (Fig. 1c) and X-ray diffraction pattern (Fig. 2), which were measured by the continuous scanning method, appear to indicate amorphous characteristics.

Before scrutinizing the conflicting results, we mention the diffraction patterns of deposits obtained from different baths. The X-ray diffraction pattern of the specimen obtained from a pH 4.9 bath shows a less sharp peak than the pH 4.6 specimen, whereas the

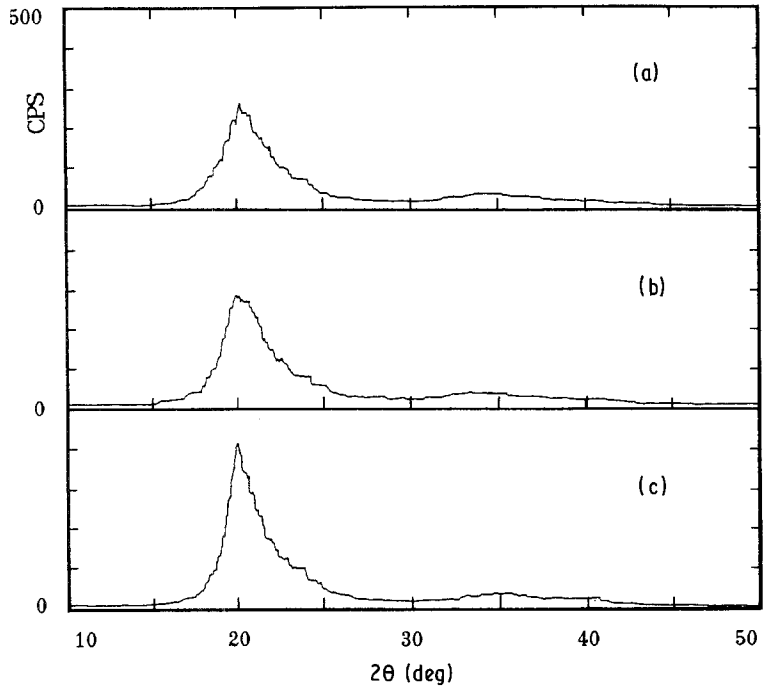

Figure 2 X-ray diffraction patterns of electroless nickel deposits obtained from (a) pH 4.6, (b) pH 4.9 and (c) pH 5.3 baths.

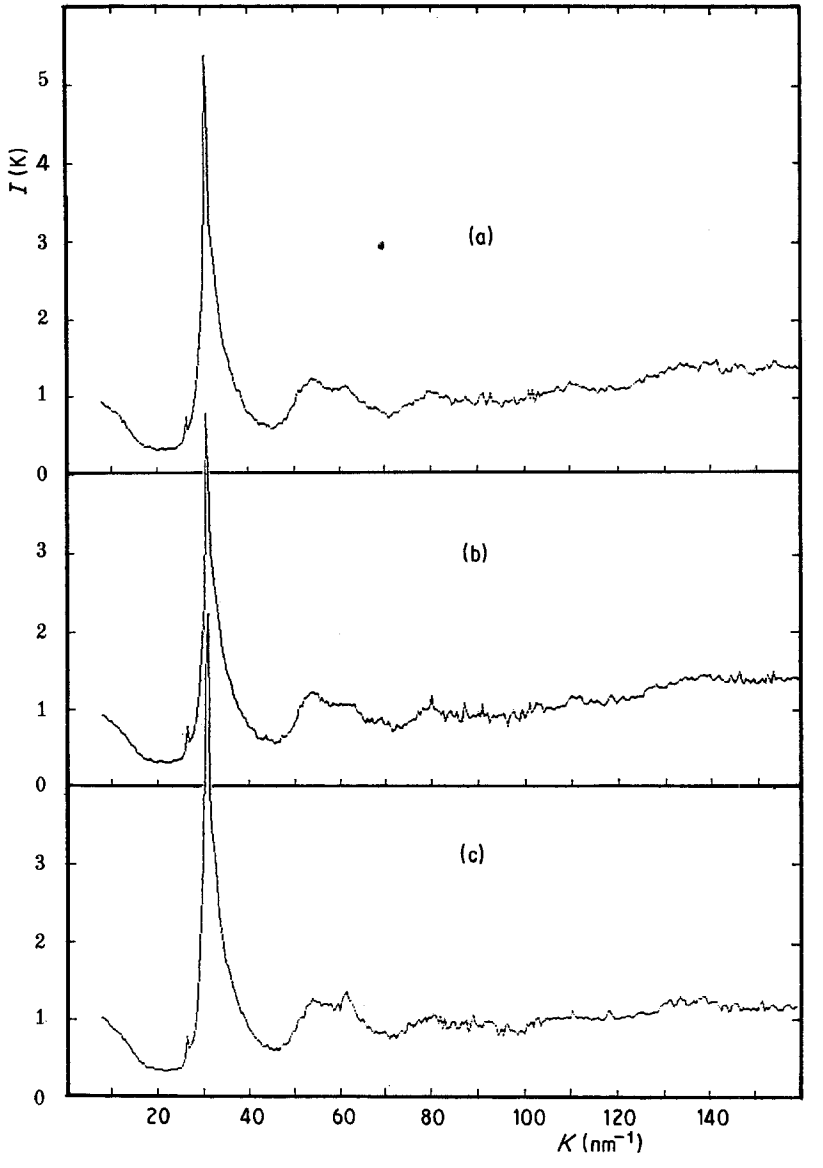

Figure 3 Interference functions of electroless nickel deposits obtained from baths at (a) pH 4.6, 10.07% P; (b) pH 4.9, 9.52% P; (c) pH 5.3, 7.42% P.

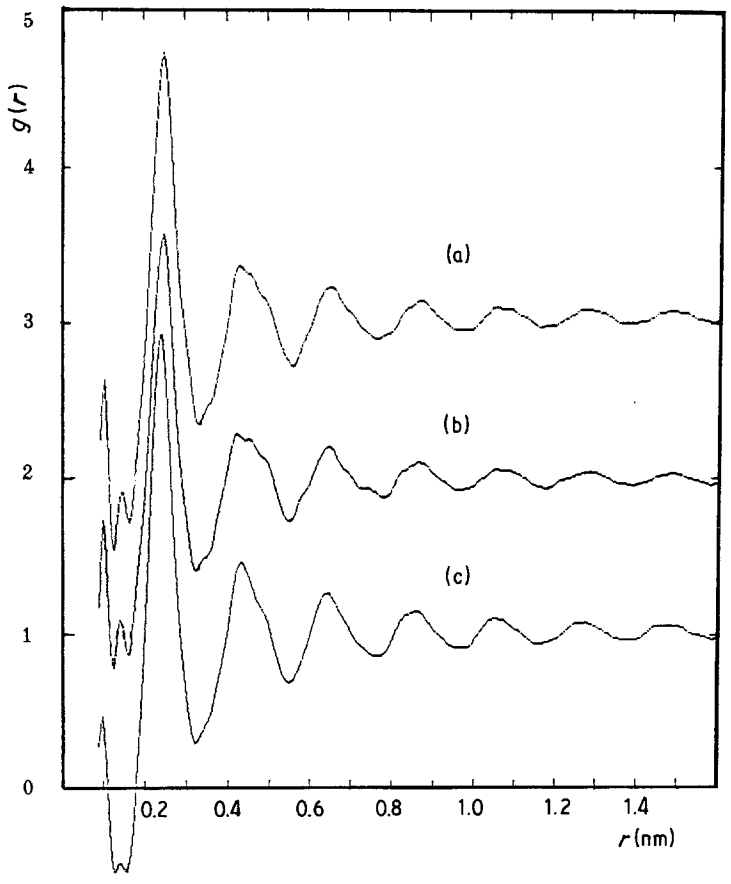

Figure 4 Pair distribution functions of electroless nickel deposits obtained from baths at (a) pH 4.6, 10.07% P; (b) pH 4.9, 9.52% P; (c) pH 5.3, 7.42% P.

pH 5.3 specimen shows a sharper peak in the diffraction pattern (Fig. 2). However, the overall shape of diffraction patterns was independent of phosphorus content. The diffraction patterns of the deposits had only a single broad peak, whose maximum diffraction angles were identical in spite of the phosphorus content variation. This may be explained by the deposit being amorphous or consisting of extremely small grains with a preferred orientation. To resolve the ambiguity, the interference function, pair distribution function and radial distribution function were calculated. Fig. 3 shows the interference functions of electroless nickel deposits with various phosphorus contents. They are almost identical except that the 7.42% P specimen has the highest first peak, followed by the 10.07% P and 9.52% P specimens in that order. It should be noted that their first-peak intensities are all higher than 4. The values are considered to be too high

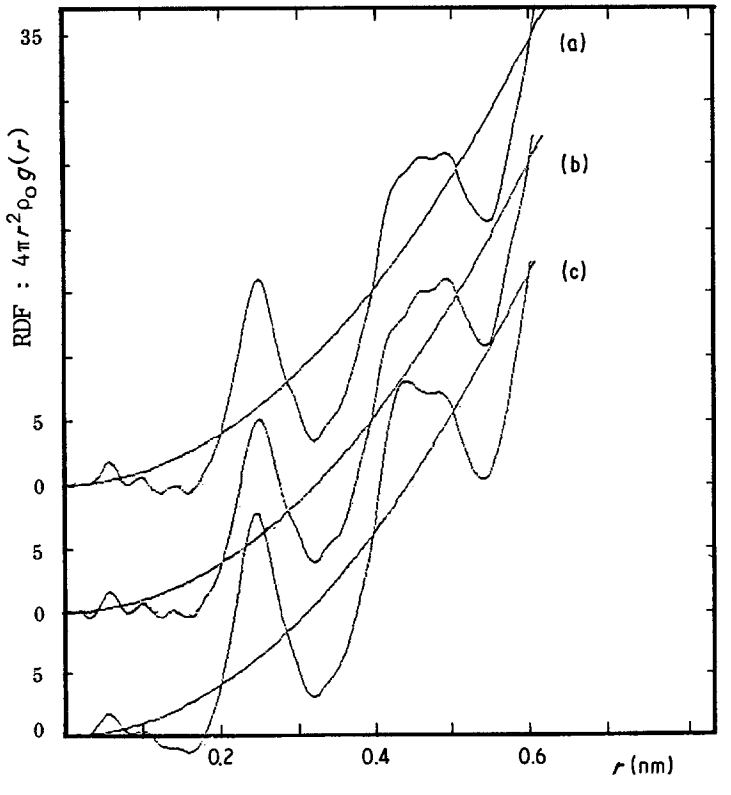

Figure 5 Radial distribution functions of electroless nickel deposits obtained from baths at (a) pH 4.6, 10.07% P; (b) pH 4.9, 9.52% P; (c) pH 5.3, 7.42% P.

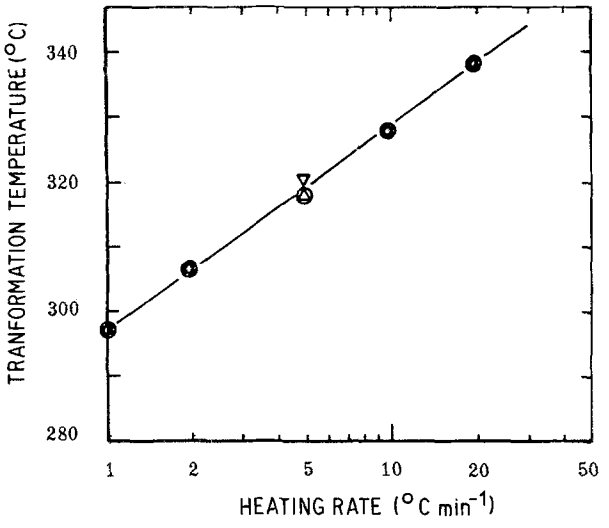

Figure 6 Effect of heating rate on phase transformation temperature of deposits at each solution pH: (○) pH 4.6, (△) pH 4.9, (▽) pH 5.3.

for amorphous materials, since the first peaks in interference function of amorphous materials are in general known to have values less than four. The pair distribution functions of the deposits (Fig. 4) indicate that crystalline characteristics were maintained up to 1.6 nm from the centre atom.

Fig. 5 shows the total radial distribution functions of the deposits, which are the Fourier-transformed values of Fig. 4. The distance from the origin to the first-peak maximum and the area of the first peak in the radial distribution function indicate the average nearest-neighbour atom distance and the coordination number, respectively. The average nearest-neighbour atom distances of samples containing 7.42, 9.52 and 10.07% P were calculated to be 0.245 29, 0.245 28 and 0.245 03 nm, and their coordination numbers 11.79, 11.64 and 11.62, which are practically the coordination number of a nickel crystal [12]. On the assumption that the deposits were a phosphorus-supersaturated solid solution of crystalline nickel, we calculated the nearest-neighbour atom distance using Vegard's law. The calculated nearest-neighbour atom distance decreased from 0.245 to 0.244 nm with increase of phosphorus content from 7.42 to 10.07%. These values are in very good agreement with the results obtained from the radial distribution function.

All the results above suggest that the deposits are phosphorus-supersaturated crystalline nickel rather than amorphous. If the deposits are crystalline, the X-ray diffraction pattern in Fig. 2 can be used to calculate the grain size using the Scherrer formula based on line broadening. The grain sizes were calculated to be 2.5 to 3.0 nm. Considering that the residual stresses developed in the specimens during plating could also provoke line broadening, which in turn made the calculated grain size finer, the grain sizes measured from the TEM microstructure (Fig. 1b) and the pair distribution functions are thought to be

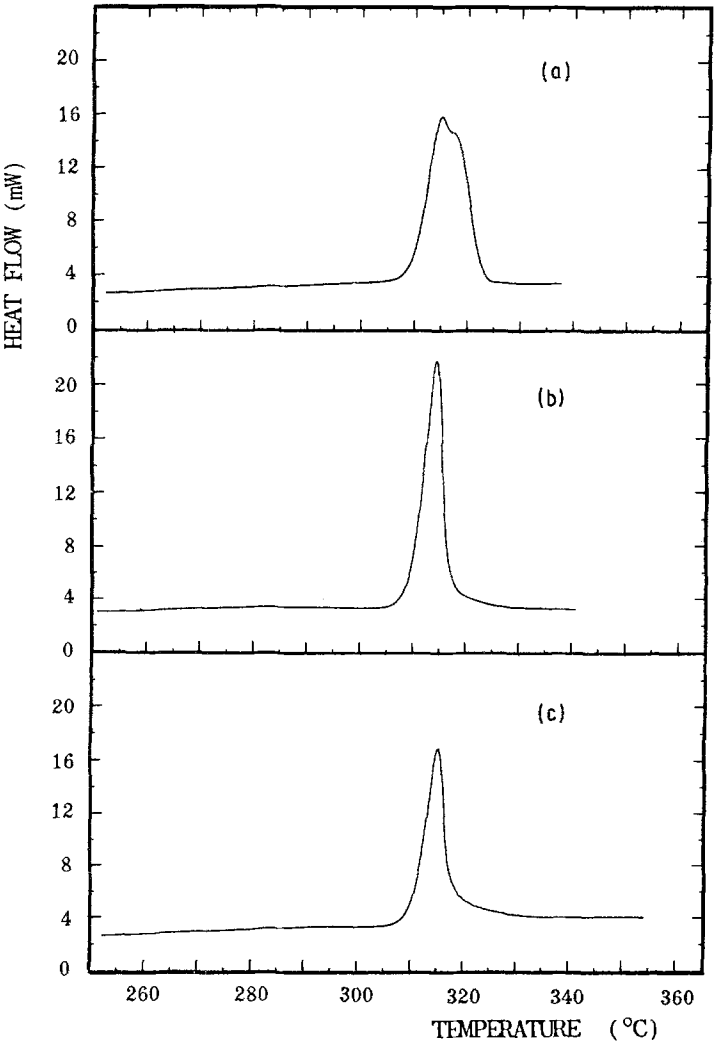

Figure 7 Phase transformation behaviour of deposits of each solution at a heating rate of 2° C min^{-1}: (a) pH 4.6, 67.3% Ni_3P: (b) pH 4.9, 63.5% Ni_3P; (c) pH 5.3, 49.5% Ni_3P.

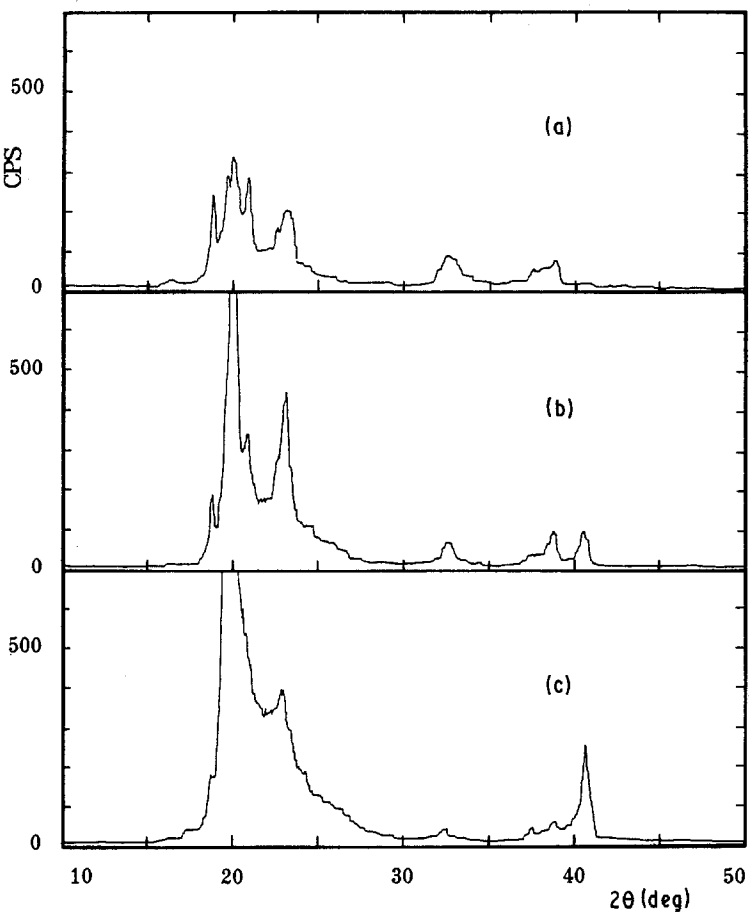

Figure 8 X-ray diffraction patterns of electroless nickel deposits annealed at 330° C for 1 h: (a) pH 4.6, (b) pH 4.9, (c) pH 5.3.

reasonable. Therefore we conclude that the electroless nickel deposits are composed of 4 to 5 nm crystallites.

3.2. Phase transformation

Fig. 6 shows the phase transformation temperature of deposits with various phosphorus contents measured using a differential scanning calorimeter and a differential thermal analyser. The transformation temperature was increased with increasing heating rate, and was independent of the pH value of the solution, and hence the phosphorus content of the specimen. Fig. 7 shows the results of thermal analysis using a differential scanning calorimeter at 2° C min^{-1} heating rate. It shows that the transformation temperature was independent of the phosphorus content of the deposit. If the electroless Ni–P deposits had an amorphous structure, a change in phosphorus content would change the transformation temperature from amorphous to crystalline. The transformation energies were calculated from the area of the peak were 38.7, 56.1 and 61.2 J g^{-1} for the 7.42, 9.52 and 10.07% P deposits respectively. These values are much smaller than the formation energy of Ni_3P from elemental phosphorus and nickel, 200 kJ mol^{-1}. It follows from the formation energy that specimens having 7.42, 9.52 and 10.07% P are calculated to require 479, 614 and 650 J g^{-1} on the assumption that all phosphorus in the specimen forms Ni_3P. These great differences between measured and calculated values may be attributed to the fact that the phosphorus atoms were already located in the interstitial sites of the crystalline nickel lattice. A shoulder after the maximum of the peak in Fig. 7a may be due to the relaxation of lattice strain energy during phase separation. The above results show that phase transformation was not due to crystallization from the amorphous material, but due to precipitation from the phosphorus-supersaturated nickel solid solution.

Microstructural changes during isothermal heat treatment at 330° C for various holding times were investigated. Figs 8 and 9 show X-ray diffraction patterns of Ni–P deposits which were heated at 330° C for 1 and 10 h respectively. After phase separation the orientation of nickel grains changed with the phosphorus content of the deposits. The orientation of the nickel grains was expressed in terms of a texture coefficient, T.C., which is defined as follows:

$$\text{T.C.} = \frac{I(hkl)/I_0(hkl)}{(1/n)\sum[I(hkl)/I_0(hkl)]}$$

where $I(hkl)$ and $I_0(hkl)$ are the integrated intensities of (hkl) reflections measured for experimental specimens and a standard powder sample, respectively, and n is the total number of reflection planes. When the T.C. of all reflection planes is unity, the distribution of crystal orientation is random. When the T.C. of any (hkl) plane is larger than unity, a preferred orientation exists in which grains are oriented with their (hkl) planes parallel to the surface. The larger the value of the T.C., the greater the degree of preferred orientation. In this study, any specimen for which T.C. $(hkl) = 4$ was determined to have all grains oriented with (hkl) planes parallel to the surface, because four reflection planes were used to calculate T.C. Table II shows the texture coefficient of nickel

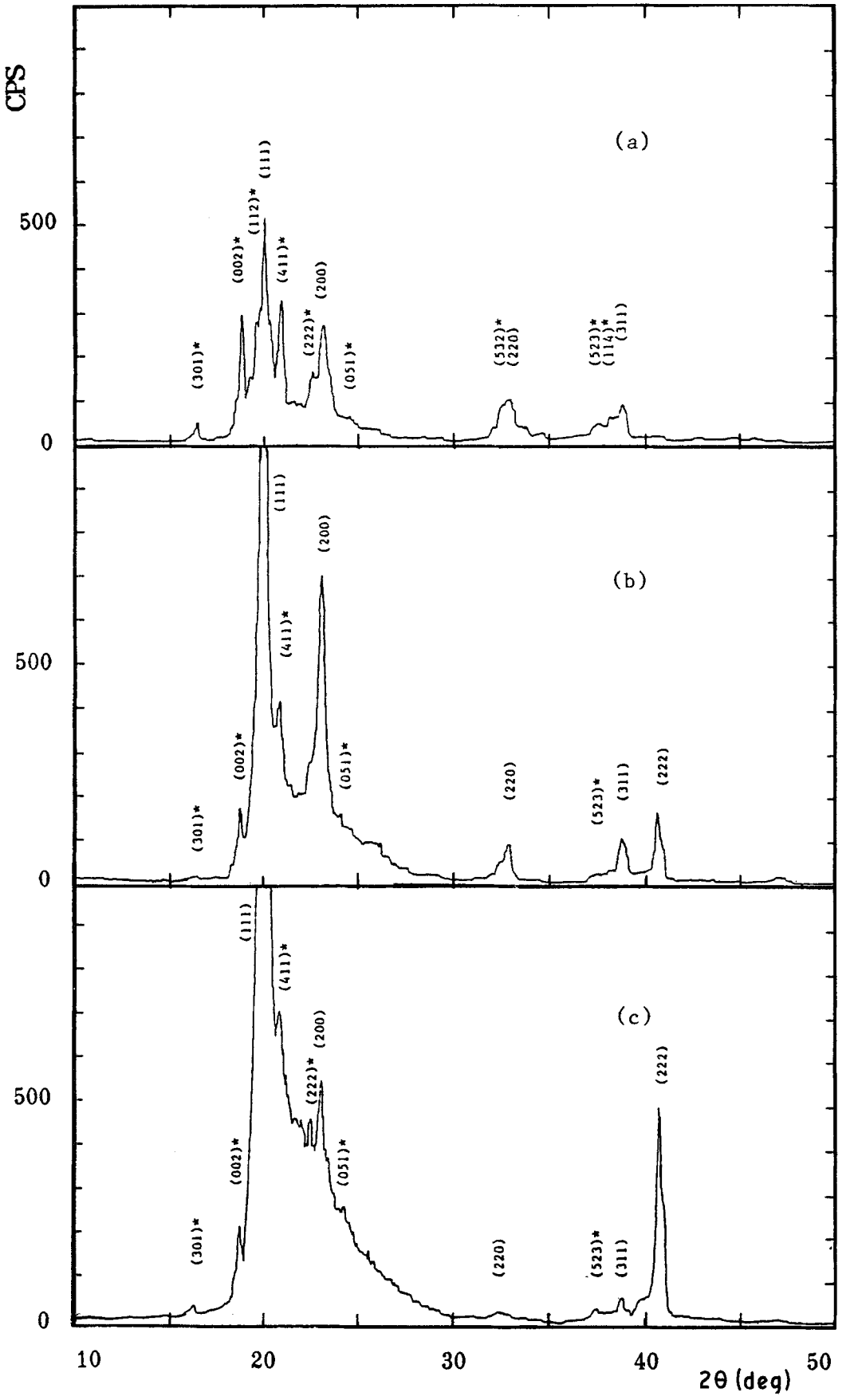

Figure 9 X-ray diffraction patterns of electroless nickel deposits annealed at 330° C for 10 h: (a) pH 4.6, (b) pH 4.9, (c) pH 5.3. (hkl) = Ni, $(hkl)^*$ = Ni_3P.

crystals calculated from Fig. 9. It shows that after heat treatment the (1 1 1) texture tended to develop as phosphorus content in the deposits decreased. If electroless Ni–P deposits had an amorphous structure, the orientation after heat treatment would be random and independent of phosphorus content. The fact that preferred orientation was developed after heat treatment shows that the electroless Ni–P deposits had a crystalline structure. In low-phosphorus Ni–P deposits (pH 5.3), which had a small fraction of Ni_3P phase, the original nickel (1 1 1) texture of the deposit was maintained even after heat treatment. The

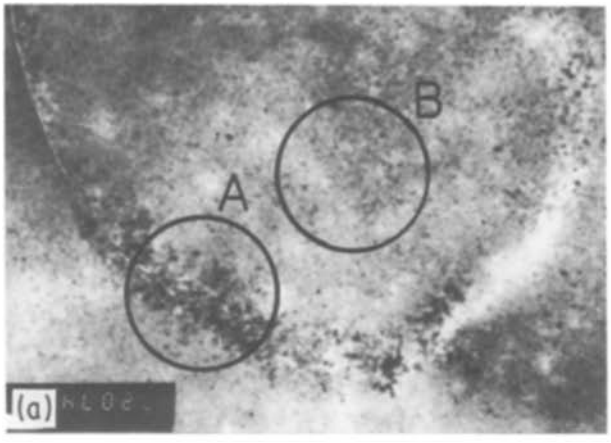

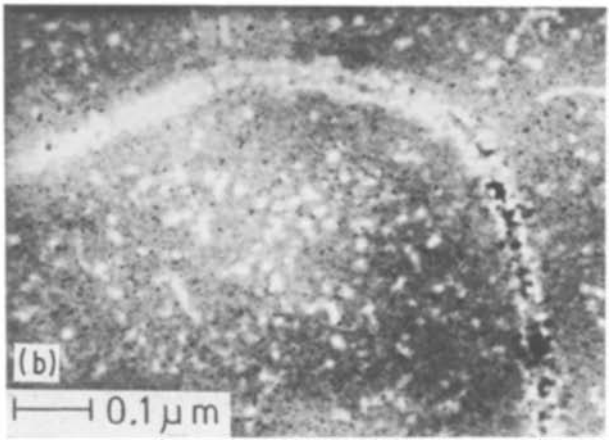

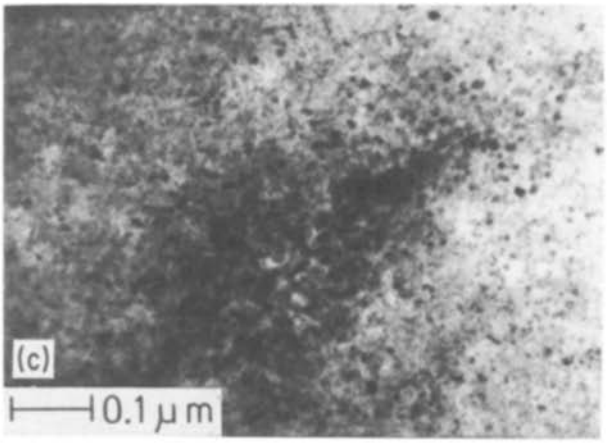

Figure 10 TEM microstructure of specimens obtained from solutions of (a) pH 4.6, (b) pH 4.9 and (c) pH 5.3, which were held in a salt bath at 330° C for 10 min.

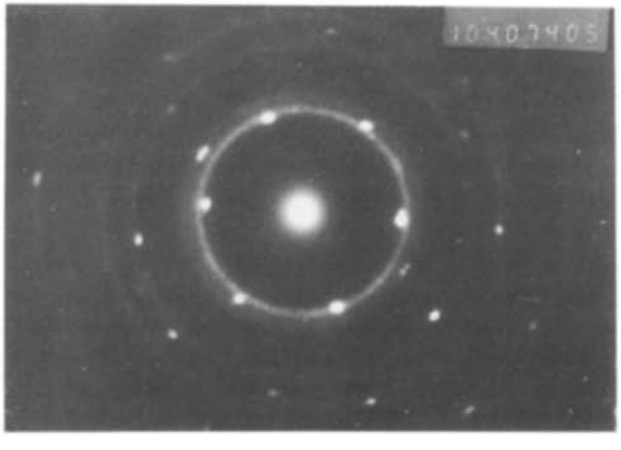

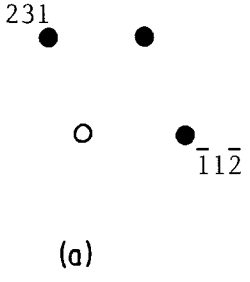

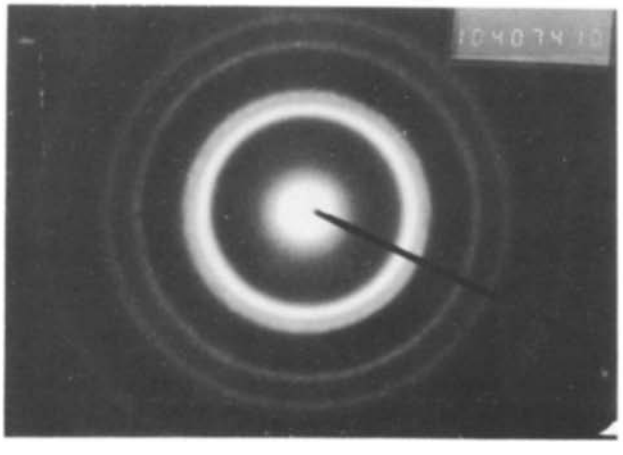

(b)

Figure 11 Selected-area diffraction patterns of (a) Region A and (b) Region B in Fig. 10a. The bright spots in (a) are from Ni_3P and the ring patterns in (a) and (b) are from nickel.

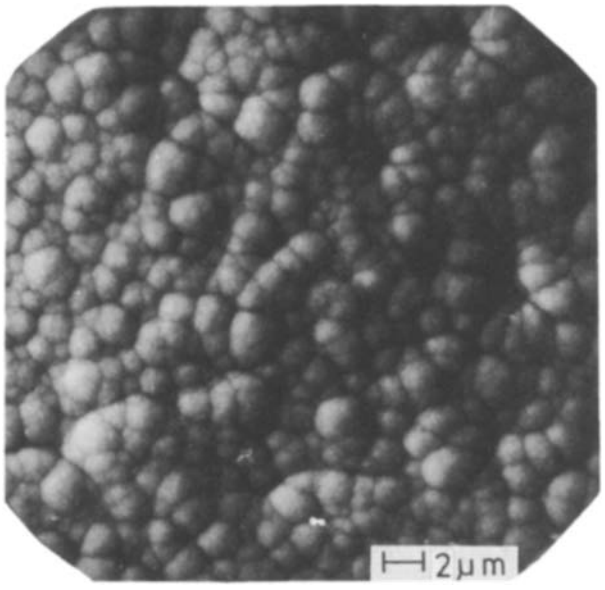

Figure 12 Scanning electron micrograph of specimen deposited for 1 h at pH 4.9.

preferred orientation of nickel crystals tends to become a random orientation with increasing phosphorus content.

Fig. 10 shows TEM microstructures of Ni–P deposits heated at 330° C for 10 min. Selected-area diffraction (SAD) patterns of regions A and B in Fig. 10a are shown in Fig. 11. The diffraction pattern in Fig. 11a shows phases of Ni_3P and nickel, whereas the pattern in Fig. 11b shows nickel only. Figs 10 and 11 indicate that an enhanced phase separation took place in Region A which is thought to be the boundary

TABLE II Texture coefficient of nickel grains in deposits obtained from solutions of various pH values, when the deposits were held in a salt bath at 330° C for 10 h

pH	Texture coefficient			
	(1 1 1)	(2 0 0)	(2 2 0)	(1 1 3)
4.6	0.96	1.16	1.0	0.88
4.9	1.91	1.31	0.35	0.43
5.3	3.37	0.56	0.06	0.01

region of deposit granules in Fig. 12. Fig. 13 shows the microstructures of Ni–P deposits after heat treatment at 330° C for 1 h. Fig. 14 shows diffraction patterns of the marked regions in Fig. 13, which are composed of sharp ring patterns of nickel and spot patterns of Ni_3P. The sharp ring pattrens came from numerous fine nickel grains, while the spot patterns came from a few Ni_3P precipitates. The Ni_3P spots near the (1 1 1) diffraction ring of nickel are slightly distorted and brighter than other spots. The results suggest that at an early stage of the phase separation Ni_3P tends to grow rapidly by encircling nickel grains, probably due to its higher grain-boundary energy, and has some coherency with the {1 1 1} planes of the nickel grains. Fig. 15a shows the (0 0 1) and (0 0 2) planes of the Ni_3P lattice in which only nickel atoms are shown. The numbered atoms in the Ni_3P lattice construct tetrahedra whose interatomic distances are shown in Fig. 15b. The tetrahedra may be thought to be distorted (1 1 1) tetrahedra of the nickel lattice. Therefore the Ni_3P phase precipitated at the early stage could have a partial coherency with neighbouring fine nickel grains. Prolonged heating would increase the quantity of Ni_3P precipitates and coarsen both them and the nickel grains (Fig. 16), which in turn would give rise to incoherency between Ni_3P and nickel crystallites as shown in Fig. 17, where the distorted brighter spots have disappeared. The higher-nickel sample from pH 5.3 solution yielded ring patterns of nickel and Ni_3P crystals when heated at 330° C for 150 min, which indicate that further heating would recrystallize the initial Ni_3P crystals. This point deserves to be studied further.

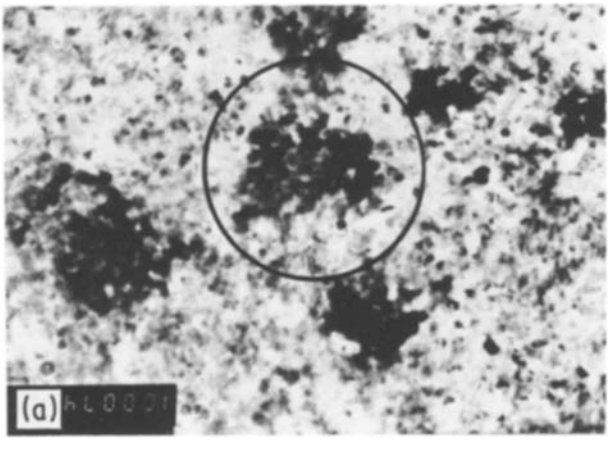

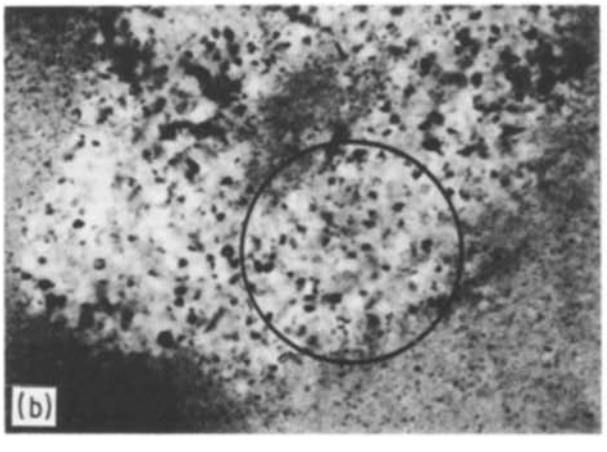

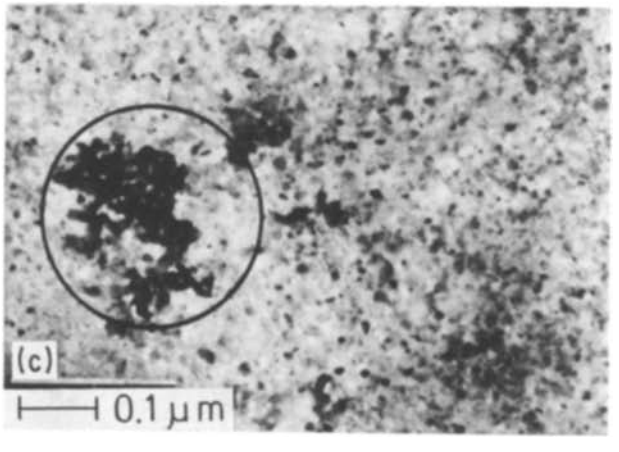

Figure 13 TEM microstructure of specimens obtained from solutions of (a) pH 4.6, (b) pH 4.9 and (c) pH 5.3, which were held in a salt bath at 330° C for 1 h.

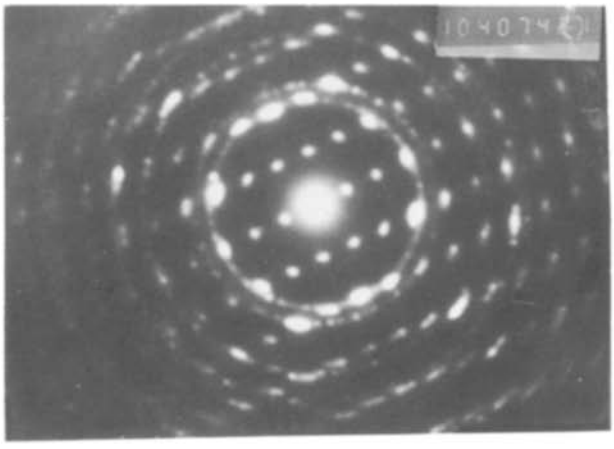

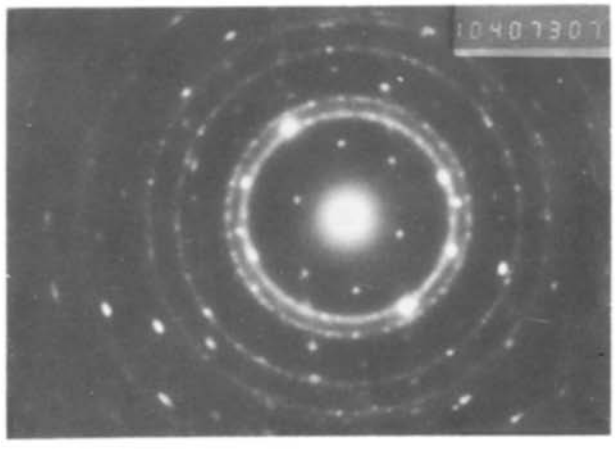

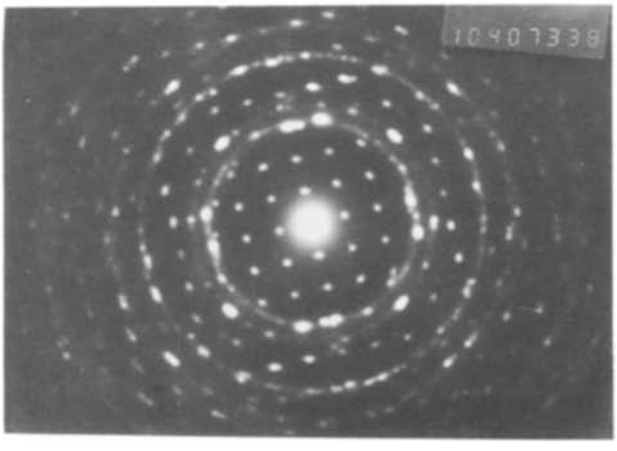

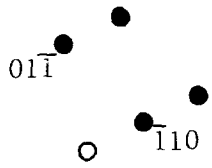

(a)

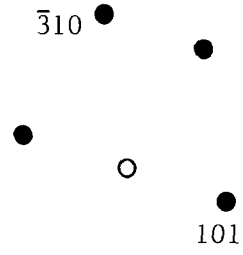

(b)

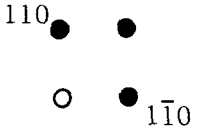

(c)

Figure 14 Selected-area diffraction patterns of marked relations in Figs 13a, b and c. Indexing is for Ni_3P.

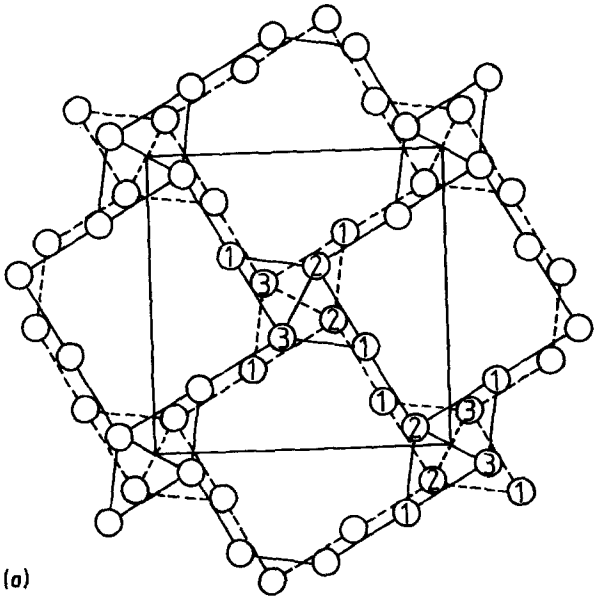

(a)

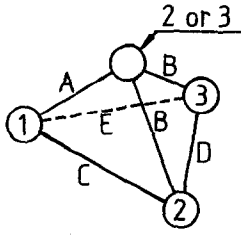

(b)

Figure 15 Schematic features of Ni_3P unit lattice. (a) planes of Ni_3P unit lattice: (——) (0 0 1) plane, (– – –) (0 0 2) plane. (b) Unit tetrahedron of nickel atoms: A = 0.252 nm, B = 0.279 nm, C = 0.285 nm, D = 0.244 nm, E = 0.260 nm.

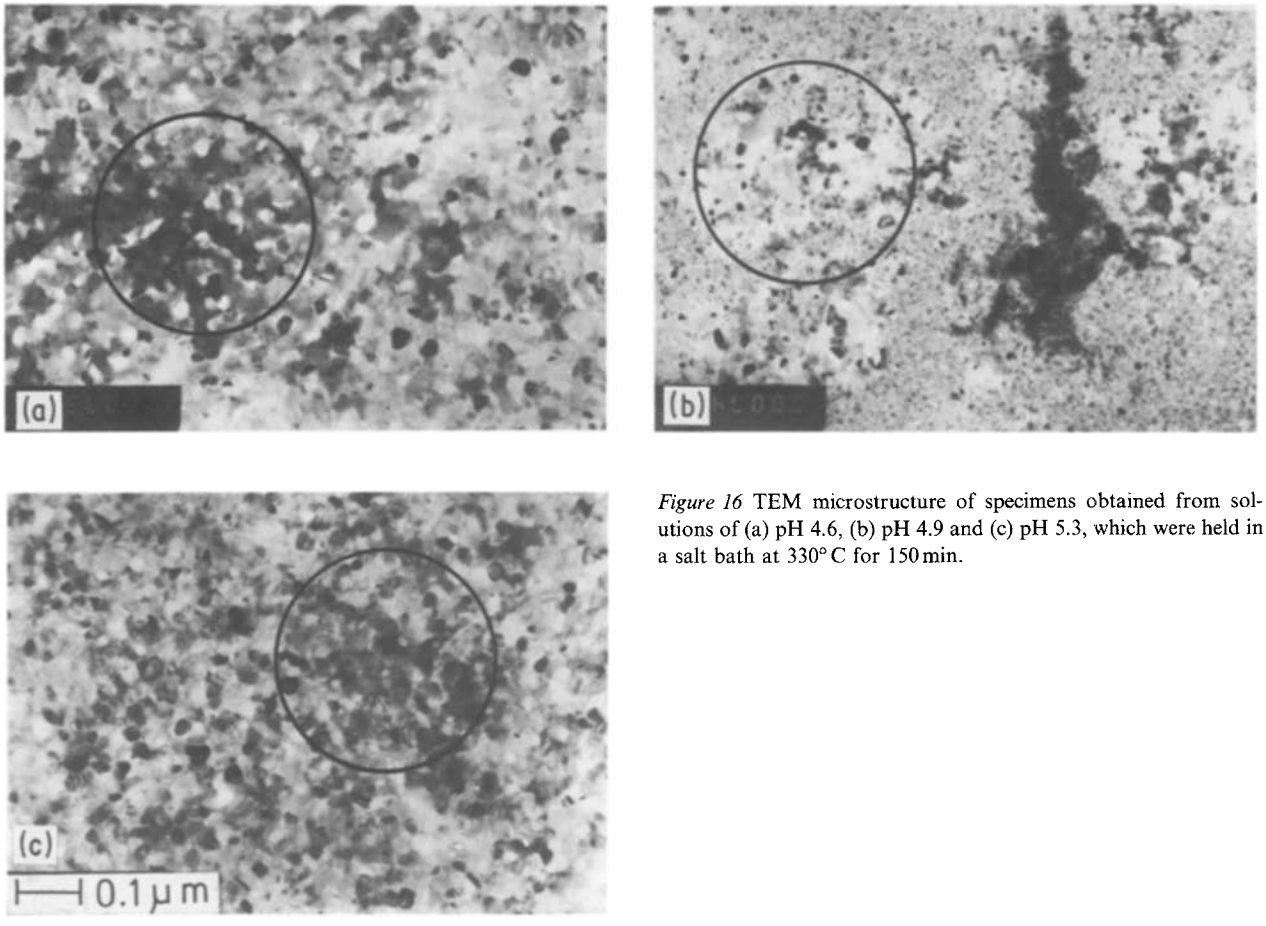

Figure 16 TEM microstructure of specimens obtained from solutions of (a) pH 4.6, (b) pH 4.9 and (c) pH 5.3, which were held in a salt bath at 330° C for 150 min.

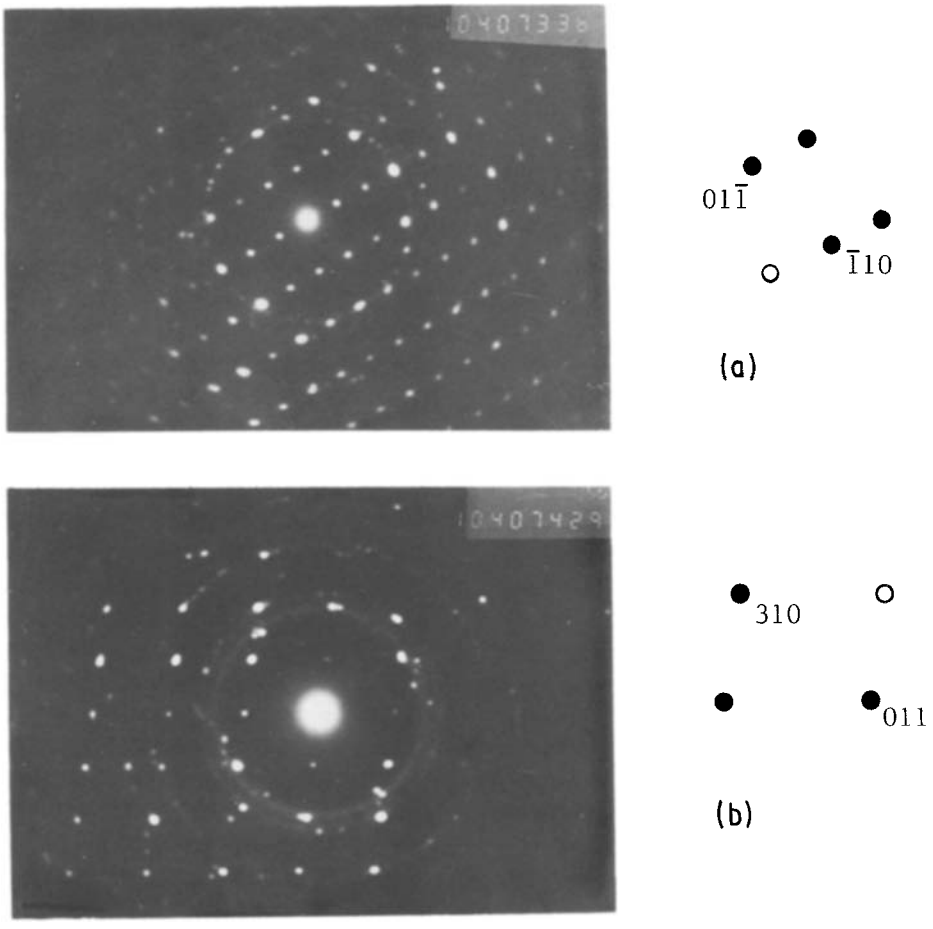

Figure 17 Selected-area diffraction patterns of marked regions in Figs 16a, b and c. Indexing in (a) and (b) is for Ni_3P, and in (c) for nickel.

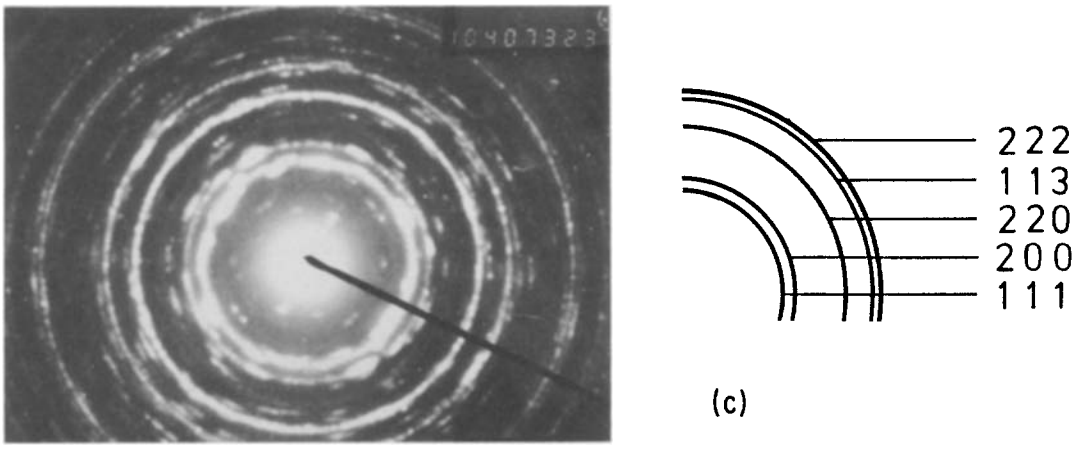

Figure 17 Continued.

4. Conclusions

The microstructure of electroless nickel deposits containing 7.4 to 10 wt % P obtained from mixtures of succinic, aminoacetic, malic and citric acid as complexing agents is a phosphorus-supersaturated nickel solid solution, whose grain size was thought to be 4 to 5 nm.

The deposits had the (1 1 1) texture of nickel grains, which was maintained even after heat treatment in the case of lower phosphorus-content deposits. As the phosphorus content in the deposits increased, the texture of nickel grains after heat treatment approached a random orientation.

The phase transformation temperature increased linearly with heating rate, but was independent of phosphorus content.

The stable phases of deposits after phase transformation were f c c nickel and b c t Ni_3P (a = 0.835 nm, c = 0.439 nm).

Acknowledgements

The authors would like to thank Il Jin Corp., Seoul, for financial support of this research. We are grateful to Mr D. W. Lee for his capable assistance in the experimental work. Also, the authors wish to acknowledge with gratitude Professor D. Y. Lee at the Department of Material Science, Korea University, Seoul, for helpful discussions on the X-ray diffraction analysis of amorphous films with a computer program, and Dr K. H. Oh at the Division of Material Science and Engineering in Korea Advanced Institute of Science and Technology, Seoul, for his valuable help in the computer calculation of radial distribution functions.

References

1. A. BRENNER and G. E. RIDDLE, US Patents 2 532 283/4 (1950).
2. C. R. SHIPLEY Jr, *Plating Surf. Finishing* **71** (June 1984) 92.
3. S. L. CHOW, N. E. HEDGECOCK, M. SCHIESINGER and J. REZEK, *J. Electrochem. Soc.* **119** (1972) 1614.
4. K. SUGITA and N. UENO, *ibid.* **131** (1984) 111.
5. A. W. GOLDENSTEIN, W. ROSTOKER, F. SCHOSSBERGER and G. GUTZEIT, *ibid.* **104** (1957) 104.
6. E. VAFAEI-MAKHSOOS, E. L. THOMAS and L. E. TOTH, *Metall. Trans.* **9A** (1978) 1449.
7. *Idem, J. Appl. Phys.* **51** (1980) 6366.
8. *Idem, J. Mater. Sci.* **16** (1981) 2103.
9. F. OGBURN, R. M. SCHOONOVER and C. E. JOHNSON, *Plating Surf. Finishing* **68** (March 1981) 45.
10. B. G. BAGLEY and D. TUNBULL, *Acta Metall.* **18** (1970) 857.
11. T. YAMASAKI, H. IZUMI and H. SUNADA, *Scripta Metall.* **15** (1981) 177.
12. Y. WASEDA and S. TAKAMI, *Z. Physik* **23** (1976) 315.
13. A. H. GRAHAM, R. W. LINDSAY and H. J. READ, *J. Electrochem. Soc.* **112** (1965) 401.
14. K. PARKER, *Plating Surf. Finishing* **68** (December 1981) 71.
15. G. S. CARGILL III, *J. Appl. Phys.* **41** (1980) 12.
16. J. DIXMIER and P. DUWEZ, *ibid.* **44** (1973) 1189.
17. G. O. MALLORY, *Plating* **61** (1974) 1005.
18. D. W. LEE, MSc thesis, Seoul National University (1985).
19. D. Y. LEE, PhD thesis, U.C.L.A. (1980).

Received 26 May
and accepted 24 July 1987